Measurement 253 (2025) 117552

Contents lists available at ScienceDirect

Measurement

journal homepage: www.elsevier.com/locate/measurement

Fast tilt compensation in non-raster rotation-scanning atomic force microscopy for improved force control and extended scanning range

Šarūnas Vaitekonis [a], Viktor Novičenko [b], Artūras Ulčinas [a,*]

[a] Department of Nanoengineering, Center for Physical Sciences and Technology (FTMC), Savanorių ave. 231, LT-02300 Vilnius, Lithuania
[b] Institute of Theoretical Physics and Astronomy, Vilnius University, Saulėtekio ave. 3, LT-10257 Vilnius, Lithuania

ARTICLE INFO

Keywords:
Atomic force microscopy
Adaptive control
High-speed atomic force microscopy
Large area

ABSTRACT

We describe an adaptive control approach for fast and efficient compensation of tilt-related variation of the interaction force between the surface and the probe of the atomic force microscope (AFM) in the case of fast rotation scanning. Apparent periodic height variation arising from the inclination between the probe's base and the surface is compensated by utilizing a recently developed technique based on a modified method of harmonic oscillators. The efficiency of the developed controller is demonstrated by achieving substantially improved interaction force control and reliable imaging at linear scanning velocities up to 3 cm/s of area of 0.19 mm^2 in 524 s with a maximum pixel size of approximately 47 nm. The ability to significantly increase the radial scanning range afforded by this method is an important step towards high-resolution, high-throughput AFM investigation of large samples.

1. Introduction

Atomic force microscopy (AFM) has become an essential tool for materials characterization at the nanoscale. Similarly to other high-resolution techniques, conventional AFM suffers from a limited field-of-view, which hinders its broad application in the technologically relevant nanofabrication contexts, where nanoscale resolution over large areas is often desired. With spectacular improvements to AFM probes, detection and control methods which enabled, for example, observation of many biomolecular systems in action [1], these limitations primarily stem from the mechanical assembly used to scan the probe with respect to the sample. The most common approach to increase the scanning speed is to make the scanning structures stiffer – which carries the penalty of reduced scanning range. Another route is to move away from the raster-scanning paradigm towards driving the scanner using the waveforms that permit to avoid sharp changes of direction, such as spiral [2], cycloid [3] or Lissajous [4].

An alternative non-raster scanning technique for AFM for large areas and high speed is inspired by the scanning systems employing combined rotational and translational motion, which had been extensively used in optical and magnetic data storage devices. In this arrangement, the sample is rotated in the plane perpendicular to the AFM probe, and the probe or the sample is translated in the radial direction so that the surface is scanned using the concentric circle or spiral trajectories. Such scanning strategy offers particular advantages in the case of samples having large mass and dimensions, as the sudden changes in acceleration related to the reversing the direction of motion are avoided, and has enabled the large area nanoscale surface investigation at high scanning speed [5,6].

Tilt is a common AFM artifact arising from the misalignment angle between the sample and the XY scanner planes (Fig. 1(a)). It may obscure the true topography of the surface if not corrected. In conventional raster-scanning AFM, the effect of the tilt is reduced by keeping the surface-probe interaction signal constant at the selected setpoint by controlling the relative probe height through the proportional-integral-derivative (PID) control circuit, with subsequent subtraction of the appropriate fit from the registered height data (flattening) [7]. The methods for tilt (and drift) removal in the case of the non-raster scanning patterns are less well-established. Meyer et al [8] used the analysis of height information from self-intersecting paths in the case of modulated Archimedean spiral and Spirograph to reconstruct the tilt and drift functions. Sun et al [9] applied a similar approach to intersecting Lissajous scanning trajectories, simplifying the analysis to the least squares method with polynomial models. Notably, in both cases, repeated scanning of the same positions on the surface is required.

Tilt becomes of particular importance when the scanning velocities are too high to efficiently maintain the control signal setpoint by PID-type control. Such a situation is encountered, for example, in fast-

* Corresponding author.

https://doi.org/10.1016/j.measurement.2025.117552
Received 7 August 2024; Received in revised form 2 April 2025; Accepted 8 April 2025
Available online 10 April 2025

scanning constant height AFM, which has found an important role in materials and biological sciences [10–12]. In this mode, PID control is usually utilized for compensation of an average height variation. As the scanning velocity increases, even this average height control may not be achievable, especially for the scanners with extended out-of-plane and in-plane scanning range which are routinely used for investigating large areas. Such scanners usually have a slower response, which can easily lead to instabilities in open-loop mode as the PID control responds to the broad range of frequencies in the sample-probe interaction signal or inadequate control in closed-loop mode. Alternatively, disregarding the influence of tilt may lead to at least two undesired consequences: 1) excessive or insufficient surface-probe interaction resulting in either the damage to the probe or the surface or the loss of information about the sample; 2) the surface-probe interaction detection sensor operating in the lower sensitivity range or outside of it altogether. In particular, for the non-raster scanning trajectories such as spiral, fast control methods operating in the narrow band or single frequency are desirable.

Here, we describe the implementation of the fast tilt compensation in non-raster rotation-scanning AFM by utilizing a recently introduced adaptive control technique operating on a single frequency (or its harmonics) based on a modified method of harmonic oscillators [13]. In contrast to the system-agnostic PID control, this method builds on the known properties of the dynamical system to achieve efficient control, as discussed further. The presented method does not require the collection of redundant information via scanning the intersecting paths. It is intended for use in high throughput and ultra-large scanning range AFM setups. Such setups would facilitate the utilization of the AFM technology in the areas where it is currently underused due to its limited throughput and field-of-view. Examples include quality monitoring in semiconductor fabrication, ranging from quality control of photomasks and surfaces at the various stages of the technological process to in-operando nanoscale testing of fabricated devices; investigation of structural change mechanisms at the nanoscale for failure-critical materials in aerospace, nuclear, and similar industries; and bioimaging for sensing and diagnostics such as DNA nanomapping [14] and skin corneocyte nanotexture imaging [15].

2. Adaptive control approach for tilt compensation

The principle of the rotation-scanning AFM is illustrated in Fig. 1(b). As the sample is rotated and translated in the radial direction, the AFM probe scans the surface following the spiral or concentric circle trajectory. During the scan, the radial position of the probe with respect to the rotation center (R) and angular (polar, Θ) position signals are acquired and converted from the polar to Cartesian (X,Y) coordinate system, which allows the construction of the image of the surface. As the AFM probe is moving away from the center of the rotation, the tilt is manifested as a periodic signal with increasing amplitude with time period corresponding to that of the angular frequency of rotation ω. The drift and surface topography features show up in the probe signal as components with significantly lower (drift) or higher (surface) frequencies (Fig. 1(c)). The aim of the tilt compensation is to eliminate the corresponding surface-probe interaction variation by adjusting the position of the Z-actuator.

Usually, this task is achieved by employing PID-type control to keep constant certain dynamic parameter of the cantilever probe representative of the probe-surface interaction, such as deflection, oscillation amplitude, resonant frequency, etc. Conventional PID does not require knowledge about, or a model of, the system to be controlled and performs adequately in cases where the rate of change of the control input is sufficiently slow compared to the dynamics of the mechanical scanner. However, as the rate of change of the control input increases, feedback-based PID control becomes increasingly challenged in terms of stability and minimization of error. In such situations, control approaches that take advantage of the insights about the dynamical system are advantageous.

In the case of rotation-scanning, the dynamical system can be treated as having a periodic orbit and producing a signal with an unknown amount of time delay, which needs to be counteracted by the controller. Provided the delay is less than a quarter of the rotation period, the control of such a system can be achieved by a linear time-invariant controller, as recently described by Novičenko and Vaitekonis [13]. Briefly, a transfer function is constructed, which uses as input the surface-probe force signal and couples this signal with a set of harmonic oscillators having natural frequencies $j\cdot\omega$, where $j = 0, 1, 2, \ldots, N$; N is limited by the Nyquist frequency:

$$C(s) = \frac{U(s)}{-X(s)} = 2\gamma\left(\frac{\alpha s + \beta\omega}{s^2 + \omega^2}\right)\left[1 + \frac{\alpha}{s} + 2\sum_{m=2}^{N}\frac{\alpha s + \beta\omega}{s^2 + m^2\omega^2}\right]^{-1} \quad (1)$$

here $X(s)$ and $U(s)$ are the Laplace transforms of the controller's input signal and the controller's output signal, respectively; the parameters α and β are the coupling constants chosen from the stability region, and γ is determined heuristically and depends on the properties of the particular system to be controlled, e.g., the detection sensitivity of the probe detection system, the stiffness of the cantilever, and so on. Coupled harmonic oscillators acquire such amplitudes and phases that their superposition begins to replicate the input signal. Then, the signal from the first oscillator is inverted and fed as a controller output having the correct amplitude and phase to compensate the first harmonic in the input signal. For practical implementation, we use the values of $\alpha = 0.1$ and $\beta =$ -0.1, which satisfy the stability criterion for the delays up to a quarter of the rotation period. The output of the controller $u(t)$ is found by solving a system of the differential equations [13]

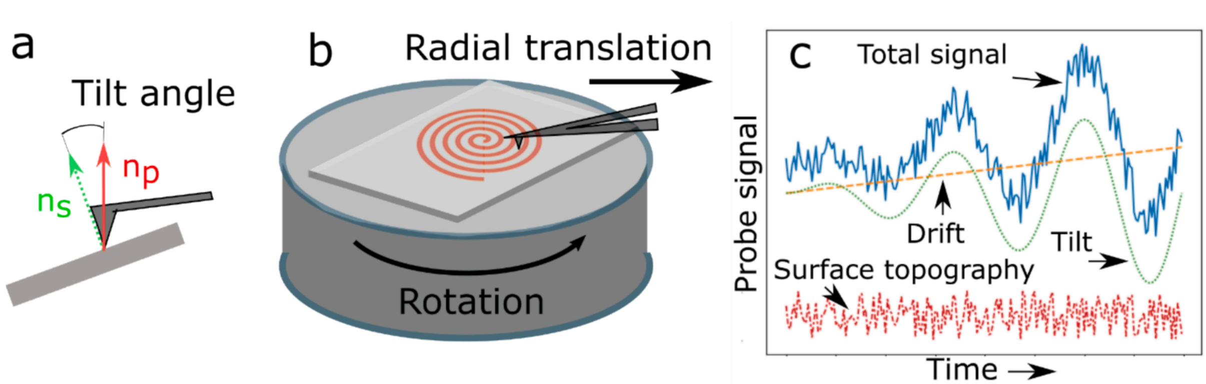

Fig. 1. (a) Illustration of the tilt between the sample and the probe: n_s – normal to the sample plane; n_p – normal to the probe scanning direction; (b) principle of rotation-scanning atomic force microscopy (AFM); (c) signal components in rotation-scanning AFM: drift (dash), tilt (dot), surface topography (dash-dot), and total signal (solid).

$$\dot{a}_0(t) = \alpha \left[x(t) - \sum_{\substack{m=0 \\ m \neq 1}}^{N} a_m(t) \right] \tag{2a}$$

$$\dot{a}_j(t) = j\omega b_j(t) + 2\alpha \left[x(t) - \sum_{\substack{m=0 \\ m \neq 1}}^{N} a_m(t) \right] \tag{2b}$$

$$\dot{b}_j(t) = -j\omega a_j(t) + 2\frac{\beta}{j} \left[x(t) - \sum_{\substack{m=0 \\ m \neq 1}}^{N} a_m(t) \right] \tag{2c}$$

here $j = 1, 2, \ldots, N$; $a_j(t)$ and $b_j(t)$ are real-value dynamical variables of the controller; $x(t)$ – state variable of the system, such as probe-surface interaction signal from the detector. The output is then calculated as

$$u(t) = -\gamma \cdot a_1(t), \tag{3}$$

and used to control the Z height of the cantilever with respect to the surface.

3. Experimental

A tilt compensation controller was implemented in an in-house developed and built digital/analog electronic board, which is directly interfaced with a PC via USB connection. The block diagram of the board is shown in Fig. 2. The central piece of the board is a mixed-signal ARM® Cortex®-M4 core microcontroller unit (MCU, STM32F303CCT6 (IC5)), STMicroelectronics) with floating point and DSP instructions running at 72 MHz. MCU has 256 K bytes of flash memory, 48 K bytes of RAM, and runs custom firmware. The board is intended to drive the external devices: the brushless direct-current (BLDC) motor to actuate the rotational motion and the Z-actuator amplifier to adjust the height of the AFM probe base. Most of the functions, such as analog-to-digital (ADC) and digital-to-analog (DAC) conversion, generation of pulse-width modulation (PWM) control signals, as well as calculation of the control output, are realized within the microcontroller (MCU).

The controller operates according to the following sequence: when the user inputs the desired rotation frequency, the suitable time base for ADC and PWM operation is calculated and set. This enables the acquisition of a fixed number of samples for processing irrespective of the rotation frequency. AFM probe signal is low-pass filtered (LPF) and sampled by the ADC. The MCU core calculates the result of the system of ordinary differential equations describing the above transfer function (Eqs (2) and (3)) in the time domain using the Adams-Bashforth linear multistep method. The calculated output is converted to the analog form and directed to the input of the Z-actuator amplifier. For direct comparison with the developed adaptive tilt compensation controller, a PID controller was implemented on the same hardware using an infinite impulse response (IIR) filter algorithm similar to that described in [16]. Values of the proportional, integral and derivative gains were manually optimized by the operator to achieve the best reduction of the first harmonic signal at a given rotation frequency. Fig. 3 shows the photograph of the developed electronic board. The computational resources in our hardware implementation were chosen for adequate operation of the compensation algorithm with a rotation frequency of up to 50 Hz.

The performance of the controller was investigated using the custom experimental AFM setup developed in-house (Fig. 4). It uses a tip-

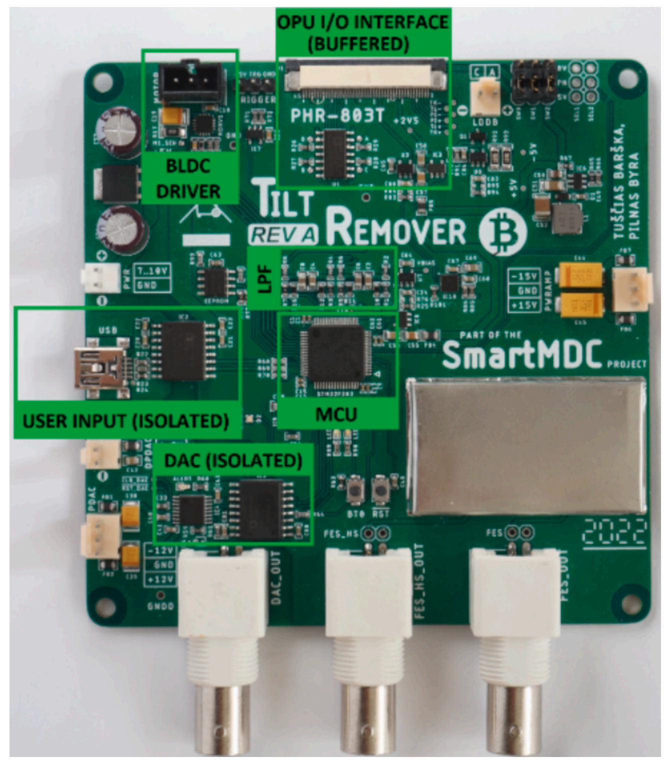

Fig. 3. Photograph of the electronic board for tilt compensation with relevant components marked and labeled: brushless direct-current (BLDC) motor driver; optical pickup unit (OPU) interface; digital-to-analog converter (DAC); microcontroller unit (MCU).

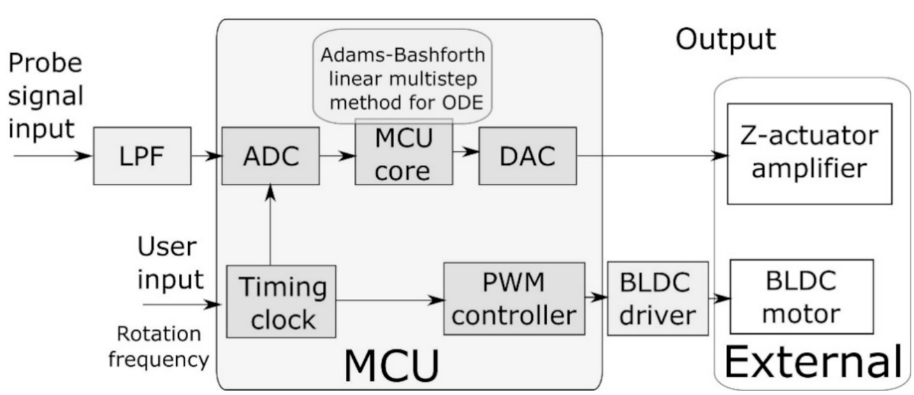

Fig. 2. Block diagram of the tilt compensation controller incorporating microcontroller unit (MCU), low-pass filter (LPF), analog-to-digital (ADC) and digital-to-analog (DAC) converters, pulse-width-modulation (PWM) controller and brushless direct-current (BLDC) motor driver.

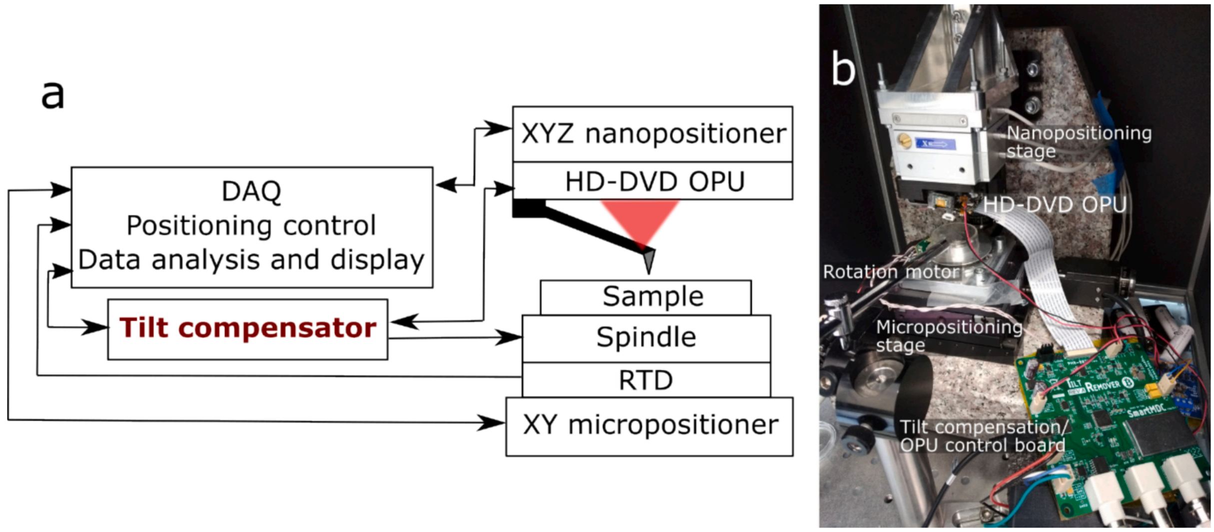

Fig. 4. Experimental rotation-scanning atomic force microscopy setup. (a) schematic block diagram; (b) photograph. HD-DVD OPU - high-definition digital versatile disk optical pickup unit; DAQ – data acquisition device; RTD – rotation tracking device. The nanopositioning stage implements radial scanning of the probe with nanometer-order precision.

scanning arrangement especially suitable for convenient investigation of the samples with large dimensions which enables nanometer precision control of both radial coordinates (X or Y) as well as possibility to use the conventional scanning approaches. We utilized a high-definition digital versatile disk (HD-DVD) optical pickup unit (OPU; PHR-803 T, Toshiba, Japan) for cantilever vertical displacement detection. This not only reduces the dimensions and mass of the detector but also enables the potential use of very small cantilevers [17]. The typical detection sensitivity factor was chosen at around 100 nm/V as determined from the linear part of the force–displacement curve taken on a hard surface, which affords a sufficient dynamic range of cantilever displacement detection of around 2 μm. Electronic circuits for controlling the laser diode and processing the photodetector signals integrated into the OPU were incorporated on the same board as the tilt compensation functionality. The OPU was mounted on an XYZ nanopositioning stage with a travel range of 51x51 μm in XY direction and 21 μm in Z (Nano-M350, Mad City Labs). The stage was operated in closed-loop mode and optimized for driving a substantial mass up to 100 g. The radial translation speed used in our experiments was 0.63–1.5 μm/s.

The rotational motion of the sample is realized by a BLDC motor removed from a hard drive and mounted on an XY motorized translation stage with a travel of 25x25 millimeters (8MT167-25, Standa). The rotation of this spindle is tracked by the chopper-type device, producing four high-to-low pulses per one revolution of the spindle. The spindle rotation frequency was found to be accurate to within 250 ppm. Furthermore, for the construction of the surface topography representation, acquired height data are analyzed for each rotation separately, thus taking into account the variation in the number of points captured during a particular rotation.

Signals corresponding to vertical displacement of the cantilever, spindle rotation tracking, and (optionally) radial position of the nanopositioning stage are sampled by a data acquisition board (NI USB-6361, National Instruments) at the rate of up to 10^6 samples per second. The data were registered and processed, and the components of the setup were controlled by the in-house developed LabView (National Instruments) virtual instrument.

AFM cantilevers used in these experiments were Multi75DLC (Budget Sensors) with the manufacturer-reported resonant frequency of 75 kHz, force constant of 5 N/m and probe radius of curvature 15 nm, and MLCT-B (Bruker, 15 kHz, 0.02 N/m, 20 nm).

4. Results and discussion

Operating the nanopositioning stage in closed-loop mode resulted in a significant phase shift between the driving signal and the final position of the Z-axis actuator at frequencies of tens of Hertz. As a consequence, satisfactory tilt compensation using conventional, non-predictive PID control at such frequencies could not be achieved. In contrast, our adaptive control technique has enabled efficient compensation of the tilt-related variation in the probe-surface force. It is worthwhile to note that one of the important advantages of our technique is that no extensive system identification or tuning is required. A single coefficient (γ in Eq.1) has to be set to a suitable value to ensure a stable operation and can be found heuristically in a straightforward way. In our experience, it is mostly dependent on two parameters: the sensitivity of the cantilever deflection detection system and the gain of the Z-actuator controller.

Comparison of the transient process as either the adaptive tilt compensation controller or PID controller is switched on is shown in Fig. 5. The probe's radial distance was approximately 50 μm from the center of rotation. The rotation frequency was set to 40 revolutions per second (rps), resulting in a travel distance of approximately 314.2 μm at a linear scanning velocity of 1.26 cm/s. The sample was a calibration grating (HS20-MG-UM, Budget Sensors) with a nominal step height of 19.5 nm. A harmonic component in the cantilever displacement signal at 40 Hz is the consequence of the effect of the tilt. Activating the adaptive tilt compensation controller leads to efficient suppression of this component by the countering action of the Z-actuator (Fig. 5(a)). At the same time, a stable PID controller achieves only a minor reduction of the tilt-related component (Fig. 5(b)). Fig. 5(c) shows the parts of the signal trace shown in Fig. 5(a, b) (marked by the dashed lines) corresponding to the cantilever displacement during one revolution period (25 ms) with either the adaptive tilt controller or PID controller on, or both controllers off; the horizontal axis in distance units is used to illustrate the distance traveled by the probe in one revolution period. With the adaptive tilt compensation, the cantilever displacement amplitude is reduced from approximately 884 nm (peak-to-peak) in the case of no tilt compensation to around 49 nm, resulting in the efficient reduction of the surface-probe force. The PID controller is significantly less efficient, reducing the amplitude only to 799 nm. Importantly, the adaptive controller does not introduce a significant disturbance into the signal related to the surface topography, as it effectively acts as a notch filter at the frequency of rotation.

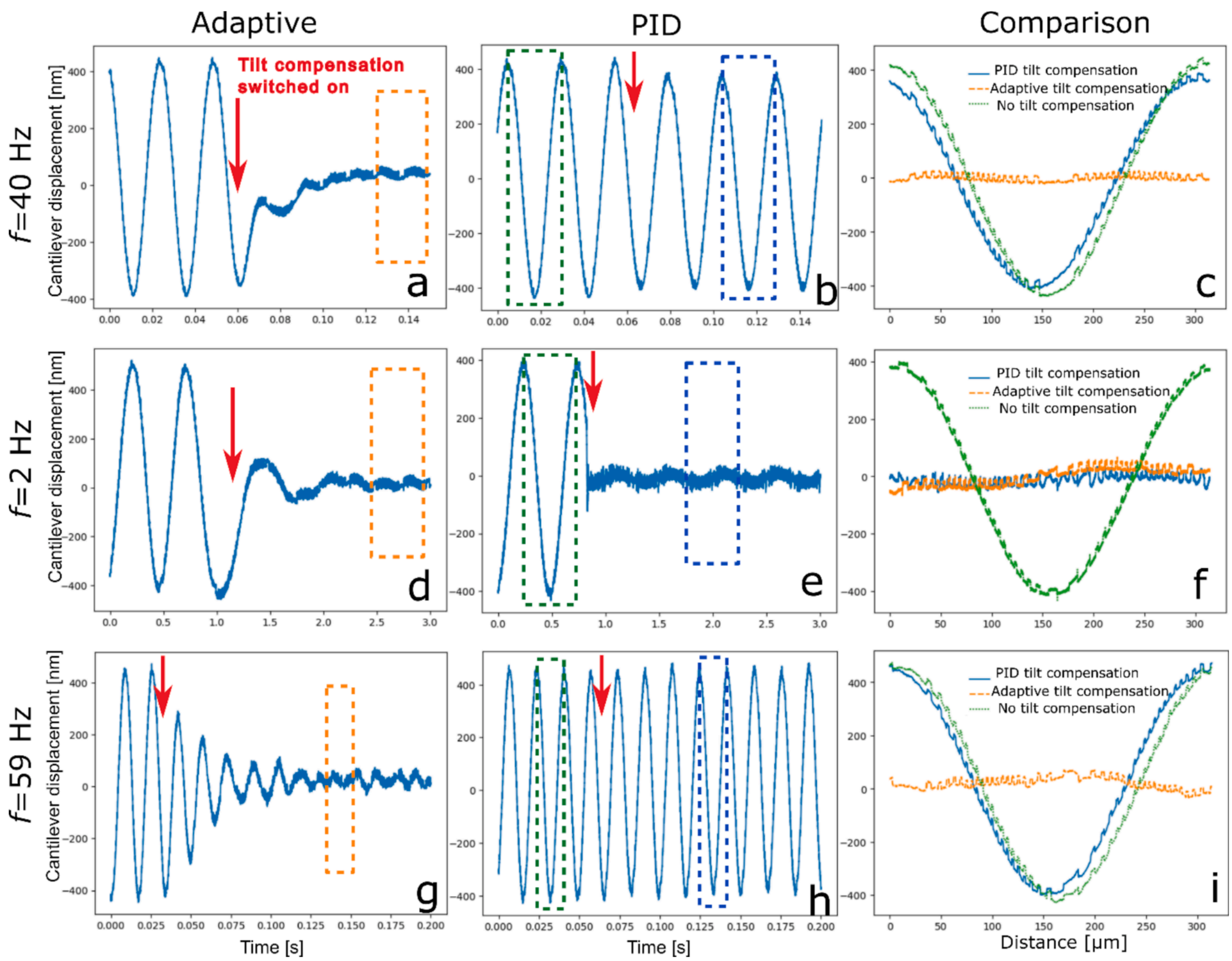

Fig. 5. The effect of compensating the influence of the probe-sample tilt using the developed control technique on the probe-surface interaction and comparison with conventional PID at different spindle rotation frequencies Traces of the cantilever signal with the tilt compensation off and on at R = 50 μm: (a-c) – 40 Hz; (d-f) – 2 Hz; (g-i) −59 Hz. Transient process after activation of the adaptive controller shows fast reduction of the tilt-related probe-surface interaction (a, d, g); (PID controller enables sufficient tilt compensation only at low rotation frequencies (e); at higher rotation frequencies PID control is ineffective (b, h). (c, f, i) Traces corresponding to one rotation period (marked by dashed lines) show the substantial reduction in the amplitude of probe-surface interaction at the rotation frequency by the adaptive controller while avoiding distortion of the signal related to the surface topography. In the case of sufficiently efficient tilt compensation using PID control, the topography representation in the cantilever displacement signal becomes distorted as PID control attempts to correct not only for tilt-related first harmonics, but also topography-related frequency (zero, first, second and so on) components in the cantilever signal.

We also compared the performance of our controller with conventional PID in two extreme cases accessible in our setup: low scanning speed at 2 rps (Fig. 5(d-f)) and high speed at 59 rps (Fig. 5(g-i)). Low speed limit in our setup is set by the reduced stability of spindle rotation, leading to jerks in spindle motion. At speeds higher than 59 rps, both the onset of undesired mechanical vibrations and eventual spindle stalling occur.

At 2 rps (linear velocity of approximately 628 μm/s) a conventional PID control is sufficiently efficient in compensating for tilt-related variation in probe-surface interaction (Fig. 5(e)). In fact, PID control settles faster than our adaptive controller (Fig. 5(f)), possibly because of the reduction in stability of the spindle motion. On the other hand, the cantilever signal, which carries the surface topography information in our setup, becomes distorted as the PID control attempts to correct not only for tilt-related, but also topography-related frequency components in the cantilever signal.

At 59 rps (linear velocity of approximately 1.9 cm/s), PID control is completely inefficient (Fig. 5(h)), while our adaptive controller is still able to significantly compensate for the tilt-related component. We note that the current speed limits are dictated by the specific hardware implementation rather than the adaptive control method itself.

To elucidate the reasons for this difference in performance between the conventional PID and our technique, we carried out their analytical comparison. Fig. 6(a) shows the frequency response of the Z-axis actuator in closed-loop mode, where solid red and blue curves represent the measured data. We approximate the Z-actuator frequency response by the second order transfer function $N(s) = (h_1 s + h_0) / (s^2 + c_1 s + c_0)$ with the values $h_1 = 92.9$; $h_0 = 403244$; $c_1 = 1297$ and $c_0 = 393903$. The frequency response of $N(s)$ is plotted in Fig. 6 by the black dashed curves. It is evident that $N(s)$ fits the measured data very well.

The block scheme of the whole system under feedback control is depicted in Fig. 6(b). The difference between the reference signal, $r(t)$, and the measured height, $x(t)$, is fed into the controller $C(s)$. The output from the controller, $u(t)$, is directed to the Z-axis actuator, $N(s)$, after which is added with the periodic signal produced by the topography and the tilt, $f(\omega t)$, and finally is applied to the cantilever, $G(s)$. Using standard notation for the Laplace transformed signals by capital letters, one can express the measured signal $X(s)$ as:

$$X(s) = R(s)\frac{C(s)N(s)G(s)}{1 + C(s)N(s)G(s)} + F(s)\frac{G(s)}{1 + C(s)N(s)G(s)}$$

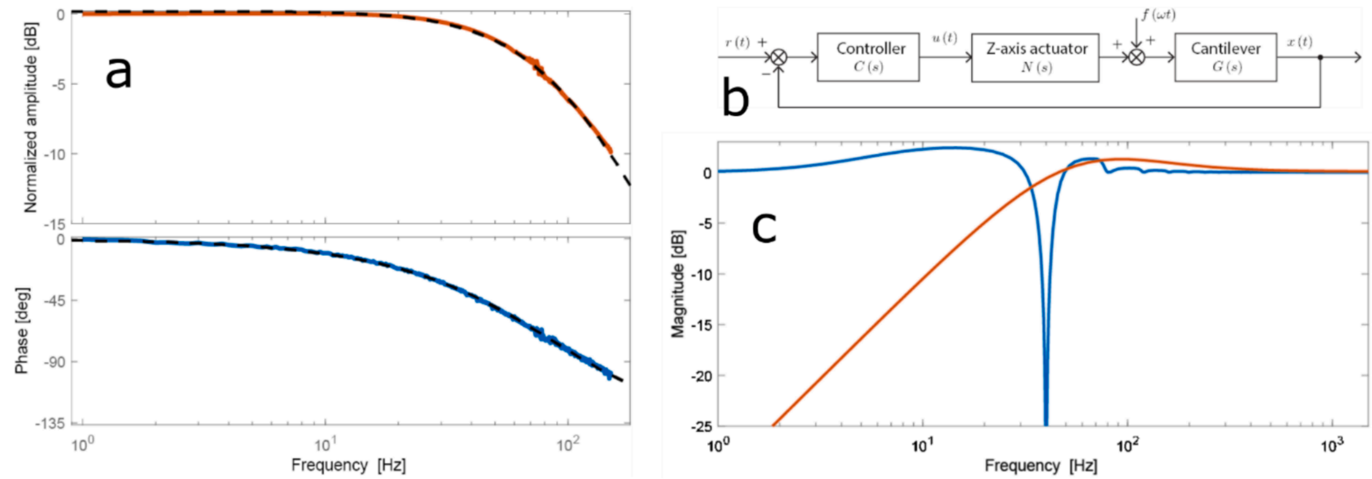

Fig. 6. Analytical comparison of PID controller and the developed technique for suppression of the tilt-related component. (a) Frequency response of the Z-axis actuator of the nanopositioning stage in closed-loop mode. Measured data (red and blue, solid) and fitted second-order transfer function (black, dashed). (b) Block diagram of the measurement system under the feedback control. (c) Frequency response of the transfer function *T(s)* responsible for the suppression of the component corresponding to the frequency of rotation at 40 Hz: our tilt compensation technique (blue line); PID controller (red). The developed technique efficiently suppresses the undesired component, whereas the PID controller is ineffective. (For interpretation of the references to colour in this figure legend, the reader is referred to the web version of this article.)

In our target frequency interval, the cantilever transfer function can be assumed to be $G(s) = 1$. Thus, the frequency response of the transfer function $T(s) = [1 + C(s)N(s)]^{-1}$ defines the gain coefficient for the first harmonic contained in the periodic signal $F(s)$. We calculated $|T(s)|$ for both cases, namely, our tilt compensation case where $C(s)$ is defined by Eq. (1) and the case of the PID controller, where $C(s) = K_I{\cdot}s^{-1} + K_p + s{\cdot}K_d$, here K_i, K_p, and K_d denote integral, proportional and derivative gains of the PID controller, respectively. The task of the PID controller is to track the reference signal $r(t)$, thus, the term next to $R(s)$ in Eq. (4) should have stable poles (the poles in the left-half side of the complex plane). Since $N(s)$ is known, using the methodology described in [18] we obtained the following optimal PID constants: $K_I = 201.1$; $K_P = 0.366$; $K_D = -9.932 \bullet 10^{-5}$. Fig. 6(c) shows the $T(s)$ frequency response for both cases: our controller (blue line) and the PID controller (red line). At 40 Hz, the developed tilt compensation algorithm reaches minus infinity, meaning that the oscillations of 40 Hz should be fully suppressed. In contrast, the PID controller has a gain factor of −0.5 dB at 40 Hz, reflecting its inefficiency in suppressing the tilt-induced component.

The main difference in efficiency between our compensation method and the PID controller is caused by the fact that they solve different tasks. While the PID controller is designed to track the reference in the broad frequency range and therefore is used in the AFM to keep a constant force of the probe-surface interaction, our technique is specifically developed to suppress particular harmonics. Once the first harmonic is removed, other frequency components remain unaffected, providing an accurate representation of probe-surface interaction.

We have investigated the influence of the efficient tilt compensation on the ability to reliably image large sample areas using the rotation-scanning AFM. Fig. 7 shows the AFM images and the line profiles of the surface of the same calibration grating sample with either the adaptive or PID tilt compensation switched on, or no compensation. Surface topography information was derived directly from the cantilever vertical displacement signal. Images were produced from the datasets with a maximum scanning radius of $R_{max} = 245$ μm captured in time of t = 524s (Fig. 7(a)), $R_{max} = 170$ μm, t = 295s (Fig. 7(b)), and $R_{max} = 140$ μm and t = 270s, respectively. The maximum distance between the samples in a dataset, and thus the attainable pixel size, was approximately 46.6 nm.

As expected, without engaging the adaptive compensation controller, the image shows a large degree of tilt as evident in the differences in the image height range (75 nm in Fig. 7(a) versus 2200 nm and 4500 nm in Fig. 7(b, c), respectively), masking the actual topography of the surface. While it is possible to remove the tilt in post-scan processing, the undesirable increase in interaction force between the probe and the surface with the scan radius may quickly lead to the negative effects discussed above, especially for fragile samples, and essentially limits the achievable scan radius. On the other hand, efficient cancellation of the tilt-related force variation enables to significantly expand the area investigated by rotation-scanning AFM.

Fig. 7(d, e, f) shows the surface topography representations of the areas indicated by the white squares on (a, b, c), respectively. Notably, the height ranges of the large area image in Fig. 7(a) and of the smaller area image in Fig. 7(d) are very similar (75 nm and 50 nm, respectively), reflecting the efficiency of the adaptive tilt compensation over the entire scanning range. Fig. 7(g, h, i) shows the line profiles taken along the lines shown in the images(d, e, f), respectively. The values of step height and pitch from the line profiles agree well with the nominal values reported by the manufacturer(19.5 nm and 10 μm). The residual variation in height seen as the alternating bright and dark lines is evident in Fig. 7 (a). We determined that this artifact is evident at higher harmonics of the spindle rotation frequency. It was found to be a consequence of the small disturbances in the motion of the BLDC motor and is not related to our tilt compensation method. This artifact is manifested at the frequency $f = M{\cdot}f_r$, where M is the number of permanent magnet pairs in the spindle and f_r, the frequency of spindle rotation. We note that the magnitude of this artifact is significantly lower than the effect of tilt.

It is worthwhile to note that even at the extreme scanning velocities used in this study (up to 3 cm/s), the efficient tilt compensation permits the AFM probe to remain in contact with the surface without applying excessive force to the surface. This allows the operator to tune the data acquisition parameters, such as sampling rate and linear and radial scanning velocity for the optimal balance between the imaging resolution, the dataset size, and the acquisition duration. At the same time, the presented technique is not designed and is not suited to correct the other sources of errors associated with high-speed scanning, e.g., sudden large magnitude changes in surface height or cantilever oscillations excited by the rapid interaction with the surface.

5. Conclusions

In conclusion, we developed and implemented a novel adaptive control method to compensate for the tilt-related variation of the probe-

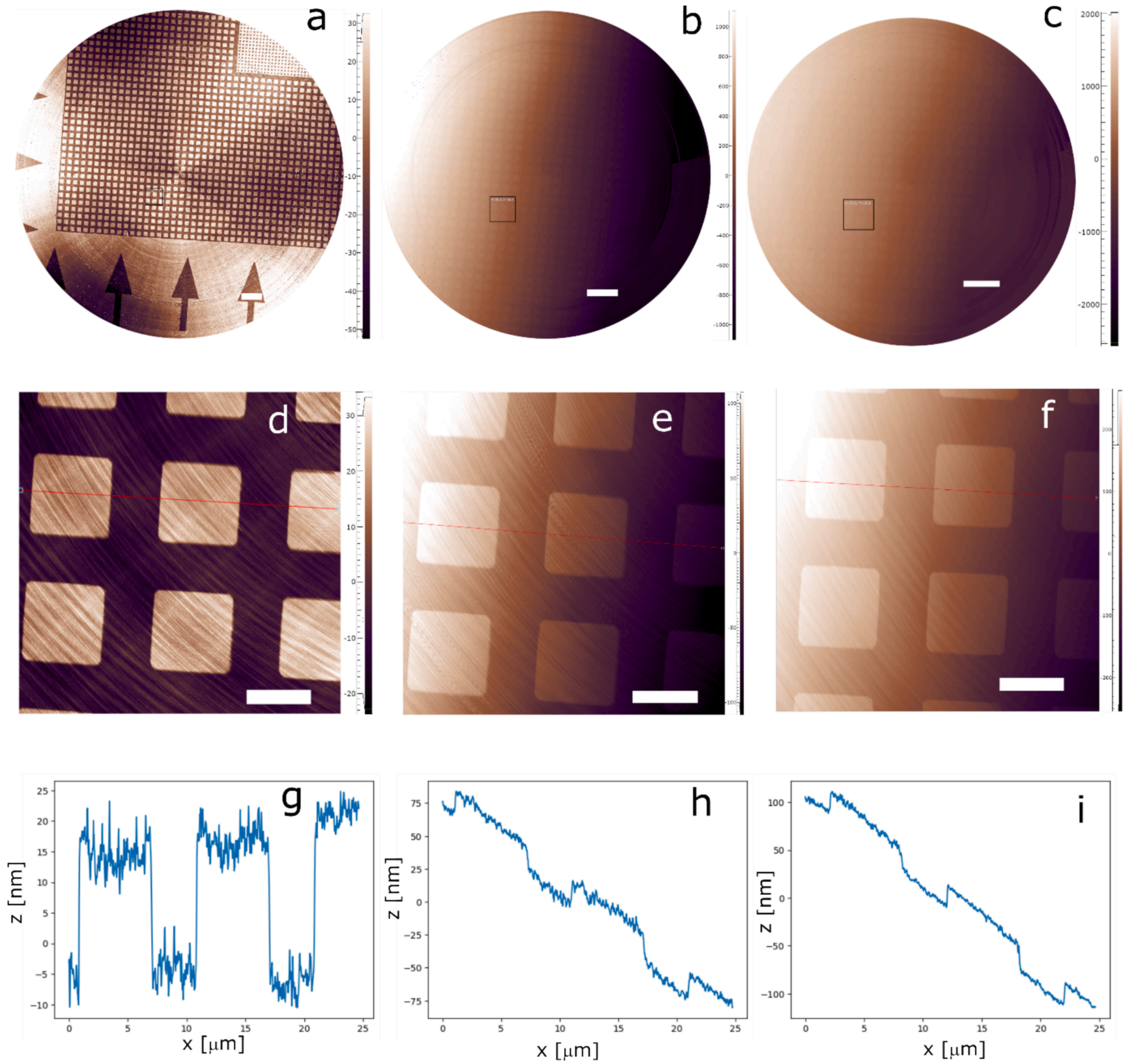

Fig. 7. Comparison of the atomic force microscopy images of the same area of the calibration grating acquired with the adaptive (a, d, g) or PID tilt controller on (b, e, h) or off (c, f, i) shows efficient removal of the tilt-related variation from the obtained height data. (a, b, c) - surface topography representation from full datasets, scalebar 30 μm; (d, e, f) - surface topography images reconstructed from the data bounded by white squares on (a, b, c), respectively; scalebar 5 μm; (g, h, i) line profiles of (d, e, f) respectively. Height range: (a) 75 nm; (b) 2200 nm; (c) 4500 nm; (d) 50 nm; (e) 200 nm; (f) 420 nm. No post-scan tilt correction was used on the acquired data. The detected height variation agrees well with the nominal grating pitch (10 μm) and height (19.5 nm) values.

surface force in fast rotation-scanning AFM. For this purpose, the developed method is preferable to the conventional PID-type control owing to its narrow band and predictive quality. The experiments demonstrate the efficiency of the method, enabling to achieve desired control of surface-probe interaction and significantly extend the radial scanning range, thus allowing to acquire ultra-large-scale AFM datasets in a reasonable time. Importantly, the tilt compensation frequency is limited primarily by the dynamic properties of the Z-actuator used to control the distance between the probe base and the sample. The method could also be applied to correct the tilt in non-raster AFM scanning approaches with orthogonal (XY) scanners, which employ driving waveforms containing single frequency [2,3], or other rotating systems where the control of the relative separation between the moving bodies is required.

CRediT authorship contribution statement

Šarūnas Vaitekonis: Writing – review & editing, Validation, Software, Methodology, Conceptualization. **Viktor Novičenko:** Writing – review & editing, Software, Methodology, Investigation, Formal analysis, Data curation, Conceptualization. **Artūras Ulčinas:** Writing – review & editing, Writing – original draft, Visualization, Validation, Supervision, Software, Resources, Project administration, Methodology, Investigation, Funding acquisition, Data curation, Conceptualization.

Declaration of competing interest

The authors declare the following financial interests/personal relationships which may be considered as potential competing interests: [Arturas Ulcinas has patent pending to Center for Physical Sciences and Technology (FTMC), and Vilnius University. Sarunas Vaitekonis has patent pending to Center for Physical Sciences and Technology (FTMC), and Vilnius University. Viktor Novicenko has patent pending to Center for Physical Sciences and Technology (FTMC), and Vilnius University. If there are other authors, they declare that they have no known competing financial interests or personal relationships that could have appeared to influence the work reported in this paper].

Data availability

Data will be made available on request.

References

[1] T. Ando, T. Uchihashi, S. Scheuring, Filming biomolecular processes by high-speed atomic force microscopy, Chem. Rev. 114 (2014) 3120–3188, https://doi.org/10.1021/cr4003837.

[2] I.A. Mahmood, S.O.R. Moheimani, Fast spiral-scan atomic force microscopy, Nanotechnology 20 (2009) 365503, https://doi.org/10.1088/0957-4484/20/36/365503.

[3] Y.K. Yong, S.O.R. Moheimani, I.R. Petersen, High-speed cycloid-scan atomic force microscopy, Nanotechnology 21 (2010) 365503, https://doi.org/10.1088/0957-4484/21/36/365503.

[4] T. Tuma, J. Lygeros, V. Kartik, A. Sebastian, A. Pantazi, High-speed multiresolution scanning probe microscopy based on Lissajous scan trajectories, Nanotechnology 23 (2012) 185501, https://doi.org/10.1088/0957-4484/23/18/185501.

[5] W. Gao, J. Aoki, B.-F. Ju, S. Kiyono, Surface profile measurement of a sinusoidal grid using an atomic force microscope on a diamond turning machine, Precis. Eng. 31 (2007) 304–309, https://doi.org/10.1016/j.precisioneng.2007.01.003.

[6] A. Ulčinas, Š. Vaitekonis, Rotational scanning atomic force microscopy, Nanotechnology 28 (2017) 10LT02, https://doi.org/10.1088/1361-6528/aa5af7.

[7] B.W. Erickson, S. Coquoz, J.D. Adams, D.J. Burns, G.E. Fantner, Large-scale analysis of high-speed atomic force microscopy data sets using adaptive image processing, Beilstein J. Nanotechnol. 3 (2012) 747–758, https://doi.org/10.3762/bjnano.3.84.

[8] T.R. Meyer, D. Ziegler, C. Brune, A. Chen, R. Farnham, N. Huynh, J.-M. Chang, A. L. Bertozzi, P.D. Ashby, Height drift correction in non-raster atomic force microscopy, Ultramicroscopy 137 (2014) 48–54, https://doi.org/10.1016/j.ultramic.2013.10.014.

[9] X. Sun, E. Heaps, A. Yacoot, Q. Yang, P. Grolich, P. Klapetek, Three-dimensional drift correction of scan data from atomic force microscopy using Lissajous scanning paths, Meas. Sci. Technol. 32 (2021) 115010, https://doi.org/10.1088/1361-6501/ac100f.

[10] L.M. Picco, L. Bozec, A. Ulcinas, D.J. Engledew, M. Antognozzi, M.A. Horton, M. J. Miles, Breaking the speed limit with atomic force microscopy, Nanotechnology 18 (2007) 044030, https://doi.org/10.1088/0957-4484/18/4/044030.

[11] L.M. Picco, P.G. Dunton, A. Ulcinas, D.J. Engledew, O. Hoshi, T. Ushiki, M.J. Miles, High-speed AFM of human chromosomes in liquid, Nanotechnology 19 (2008) 384018, https://doi.org/10.1088/0957-4484/19/38/384018.

[12] A. Mikheikin, A. Olsen, K. Leslie, F. Russell-Pavier, A. Yacoot, L. Picco, O. Payton, A. Toor, A. Chesney, J.K. Gimzewski, B. Mishra, J. Reed, DNA nanomapping using CRISPR-Cas9 as a programmable nanoparticle, Nat Commun 8 (2017) 1665, https://doi.org/10.1038/s41467-017-01891-9.

[13] V. Novičenko, Š. Vaitekonis, Controller for rejection of the first harmonic in periodic signal with uncertain delay, (2024). https://doi.org/10.48550/arXiv.2403.11731.

[14] S.R. Koebley, A. Mikheikin, K. Leslie, D. Guest, W. McConnell-Wells, J.H. Lehman, T. Al Juhaishi, X. Zhang, C.H. Roberts, L. Picco, A. Toor, A. Chesney, J. Reed, Digital polymerase chain reaction paired with high-speed atomic force microscopy for quantitation and length analysis of DNA length polymorphisms, ACS Nano 14 (2020) 15385–15393, https://doi.org/10.1021/acsnano.0c05897.

[15] H.-S. Liao, I. Akhtar, C. Werner, R. Slipets, J. Pereda, J.-H. Wang, E. Raun, L. O. Nørgaard, F.E. Dons, E.E.T. Hwu, Open-source controller for low-cost and high-speed atomic force microscopy imaging of skin corneocyte nanotextures, HardwareX 12 (2022), https://doi.org/10.1016/j.ohx.2022.e00341.

[16] https://en.wikipedia.org/wiki/Proportional–integral–derivative_controller#Pseudocode.

[17] A. Ulčinas, L.M. Picco, M. Berry, J.K. Heinrich Hörber, M.J. Miles, Detection and photothermal actuation of microcantilever oscillations in air and liquid using a modified DVD optical pickup, Sensors and Actuators A: Physical 248 (2016) 6–9, https://doi.org/10.1016/j.sna.2016.07.007.

[18] K.J. Åström, T. Hägglund, Advanced PID control, Systems and Automation Society, ISA - The Instrumentation, 2006 http://lup.lub.lu.se/record/535630 (accessed September 20, 2024.